Measurement of Rotordynamic Coefficients for a Hydrostatic Radial Bearing

B. T. Murphy

M. N. Wagner

Rockwell International,
Rocketdyne Division,
Canoga Park, CA 91304

Measurement of rotordynamic coefficients is presented for a pair of hydrostatic radial bearings, including direct and cross-coupled stiffness and damping. Two different hydrostatic configurations were tested: (1) an externally fed bearing 74.7 mm (2.95 in.) in diameter with a nominal direct stiffness of approximately 210 MN/m (1.2 million lb/in.) and (2) an internally fed bearing 54.6 mm (2.15 in.) in diameter with a nominal direct stiffness of approximately 88 MN/m (0.5 million lb/in.). Each bearing had 6 equally spaced hydrostatic pressure pockets, stationary for the externally fed bearing and rotating for the internally fed bearing. Also, both bearings had extended exit regions to provide additional damping. The top rotational speed was 22,700 rpm and the maximum axial Reynolds number was 50,000 using a freon derivative, Freon-113, as the working fluid. The test apparatus was a "synchronous rig" as an intentionally eccentric journal was used as the sole source of excitation. Data reduction was done by performing a matrix solution to separate damping from stiffness. Results show the internally fed bearing to be 20 percent less stiff than predicted, and to have a significant amount of damping which agrees well with predictions. The internally fed bearing was found to be approximately 60 percent less stiff than predicted, and to be roughly neutral in terms of damping, as predicted.

Introduction

The ball bearings which support the rotating shafts of the SSME high-pressure turbopumps have demonstrated their reliability based on numerous hot-fire tests and actual flights of the Space Shuttle. However, one of the major goals for upgrading the performance of the SSME is to increase the life of the high pressure oxidizer turbopump bearings beyond the current one mission limit. These bearings operate at extremely high DN values, and also react very large static and dynamic loads. Numerous design modifications have been made to the high-pressure turbopumps to effectively increase the bearing capacity, and reduce loads. As part of this effort to extend turbopump bearing life, the work reported here describes test results obtained on high-speed, high-pressure, liquid-fed hydrostatic bearings. The potential application of a hydrostatic bearing to turbopump technology is three-fold: (1) it can produce extremely high stiffness which can be used as a long-life replacement for mechanical element bearings, (2) it can be used as a load sharing device when used in conjunction with a mechanical bearing, and (3) through proper design, it can be an effective damping device, thereby reducing dynamic bearing loads and increasing rotor stability.

Contributed by the Tribology Division of THE AMERICAN SOCIETY OF MECHANICAL ENGINEERS and presented at the Joint ASME/STLE Tribology Conference, Toronto, Canada, October 7–10. Manuscript received by the Tribology Division February 26, 1990; revised manuscript received June 26, 1990. Paper No. 90-Trib-31. Associate Editor: I. Green.

The hydrostatic bearing test apparatus has been designed, fabricated, and used to measure the rotordynamic stiffness and damping, both direct and cross-coupled, for two kinds of hydrostatic bearings: an externally fed bearing, and an internally fed bearing. A high density Freon derivative was used as a surrogate fluid due to its hydrodynamic similarity to cryogenic turbopump propellants. Forced dynamic motion across the bearing fluid film is generated by mounting the bearing journal eccentrically on the test shaft (see Fig. 1). Thus, the test apparatus is operated with a synchronous excitation only. The relative whirl orbits across the fluid film are made to be elliptic with asymmetric stiffness in the test bearing's supporting structure. This elliptic nature is utilized in the data reduction process.

Other test results for a hydrostatic bearing have been reported by Goodwin et al. Their experiments were for a hydrostatic supported journal bearing, and do not apply to the types of configurations tested here. No other test results, particularly direct damping, have been noted in the literature for these types of bearings.

Method of Measurement

The test method for determining dynamic coefficients of hydrostatic bearings involves generating a forced dynamic motion across the bearing fluid film, and measuring the resulting fluid film displacements and forces. These displacements and

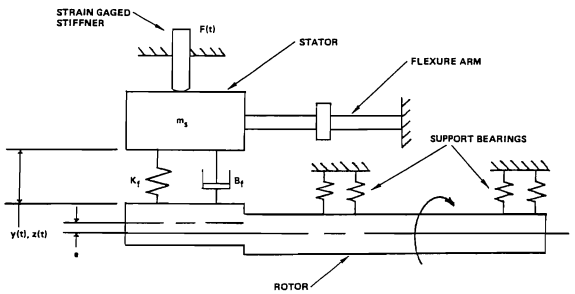

Fig. 1 Measurement technique for hydrostatic bearing tester using an eccentric journal to provide synchronous excitation

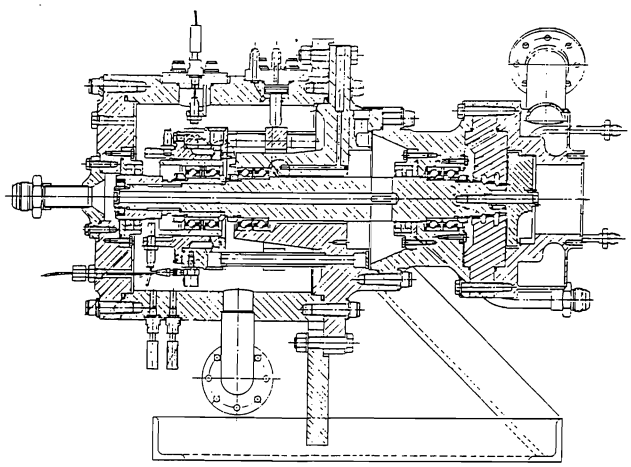

Fig. 2 Cross section of tester. Test element shown is a hybrid bearing with ball and hydrostatic bearings in series (not tested).

forces provide the means for computing the rotordynamic coefficients.

The forced dynamic motion is generated as depicted in Fig. 1. The overhung test bearing is located on the outboard end of a test shaft supported by two duplex pair of ball bearings (see also Fig. 2). The rotating part of the test bearing has been given an intentional eccentricity (i.e., runout) at the test bearing location. When the shaft rotates, the eccentricity generates an orbital pattern synchronous with shaft speed. This orbital pattern is measured with a pair of eddy current displacement probes mounted directly in the stator of the test bearing (see Fig. 3). In this way, with the stator element in motion, the displacement probes will directly measure the desired relative deflection across the fluid film.

The stator element is supported by eight tubes (flexure arms), one of which is shown in Fig. 1. These tubes supply fluid to the externally fed test bearing. In addition to the stiffness of the flexure arms, the stator element is elastically constrained in the radial direction by two pair of preloaded strain gaged load cells (see Figs. 1 and 2). The load cells were calibrated for load sensitivity and stiffness by applying known static loads directly to the stator at midplane of the test bearing. Under test conditions, the strain gage readings reflect the sum of the fluid film forces and the inertia force of the stator mass. As data reduction to rotordynamic coefficients requires the fluid film force by itself, the stator inertia force must be subtracted from the load cell readings. With the mass of the stator known, this is done as follows:

$$F_y = -\bar{F}_y + m_s(d^2/dt^2)(-\bar{F}_y/K_{sy}) \quad (1)$$

$$F_z = -\bar{F}_z + m_s(d^2/dt^2)(-\bar{F}_z/K_{sz}) \quad (2)$$

where

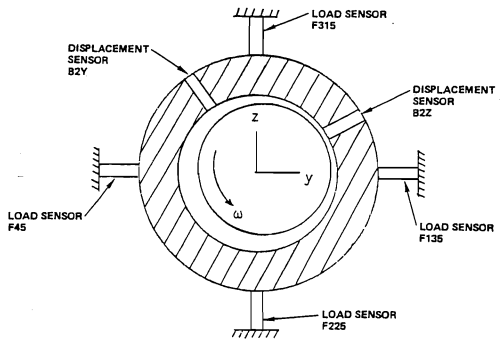

Fig. 3 Arrangement of load and displacement sensing devices. The stator is flexibly supported by four preloaded load sensors.

$\bar{F}_{y,z}$ = components of load cell reaction force acting on stator
$F_{y,z}$ = components of fluid film force acting on stator
m_s = stator mass
$K_{sy,sz}$ = stator support stiffness, can be asymmetric

The technique of using strain gage load data to compute the inertia term was found equally effective to using stator mounted accelerometers, and was employed here since it involves processing fewer data channels.

Since the shaft is driven with a synchronous harmonic load, the resulting shaft motion will, in general, be elliptic. Therefore, the goal of the measurement process is to identify the ellipse that describes the relative displacement as a function of time in the following form (relative = rotor − stator):

$$y(t) = a(\cos\omega t) + b(\sin\omega t) \quad (3)$$

$$z(t) = g(\cos\omega t) + h(\sin\omega t) \quad (4)$$

The four coefficients "*abgh*" are termed Fourier coefficients, and ω is the tester speed in radians per second. They are obtained from the synchronous components of complex frequency spectrums computed for the y and z displacements.

The same procedure is applied to the load data to obtain Fourier coefficients in the following form:

$$\bar{F}_y = \bar{m}(\cos\omega t) + \bar{n}(\sin\omega t) \quad (5)$$

$$\bar{F}_z = \bar{p}(\cos\omega t) + \bar{q}(\sin\omega t) \quad (6)$$

The equations correcting for stator inertia are then:

$$F_y = -[\bar{m}(\cos\omega t)+\bar{n}(\sin\omega t)] + (m_s/K_{sy})(\bar{m}\omega^2(\cos\omega t)+\bar{n}\omega^2(\sin\omega t)) \quad (7)$$

$$F_z = -[\bar{p}(\cos\omega t)+\bar{q}(\sin\omega t)] + (m_s/K_{sz})(\bar{p}\omega^2(\cos\omega t)+\bar{q}\omega^2(\sin\omega t)) \quad (8)$$

or

$$F_y = m(\cos\omega t) + n(\sin\omega t) \quad (9)$$

$$F_z = p(\cos\omega t) + q(\sin\omega t) \quad (10)$$

where

$m = \bar{m}(-1+(m_s\omega^2/K_{sy}))$ etc.
$mnpq$ = Fourier coefficients for fluid film force (acting on stator)

With the fluid film force and displacement now specified as functions of time, rotordynamic coefficients can be computed. The relationship between these three sets of quantities is:

$$\begin{Bmatrix} F_y \\ F_z \end{Bmatrix} = \begin{bmatrix} K_{yy} & K_{yz} \\ K_{zy} & K_{zz} \end{bmatrix} \begin{Bmatrix} y \\ z \end{Bmatrix} + \begin{bmatrix} B_{yy} & B_{yz} \\ B_{zy} & B_{zz} \end{bmatrix} \begin{Bmatrix} \dot{y} \\ \dot{z} \end{Bmatrix} + \begin{bmatrix} M_{yy} & M_{yz} \\ M_{zy} & M_{zz} \end{bmatrix} \begin{Bmatrix} \ddot{y} \\ \ddot{z} \end{Bmatrix} \quad (11)$$

The displacements and forces were defined above using

Fourier coefficients. The velocities and accelerations are obtained by differentiation with respect to time. Note that the measured force and displacement orbits will vary with tester rotational speed, and complete sets of Fourier coefficients can be made available for any speed within the tester's speed range. Two approaches were employed to calculate rotordynamic stiffness and damping from the data. One approach is to drop the inertia terms and rearrange equation (11) as follows:

$$\begin{bmatrix} b\omega & h\omega & a & g & 0 & 0 & 0 & 0 \\ -a\omega & -g\omega & b & h & 0 & 0 & 0 & 0 \\ 0 & 0 & 0 & 0 & b\omega & h\omega & a & g \\ 0 & 0 & 0 & 0 & -a\omega & -g\omega & b & h \end{bmatrix} \begin{Bmatrix} B_{yy} \\ B_{yz} \\ K_{yy} \\ K_{yz} \\ B_{zy} \\ B_{zz} \\ K_{zy} \\ K_{zz} \end{Bmatrix} = \begin{Bmatrix} m \\ n \\ p \\ q \end{Bmatrix} \tag{12}$$

Since data from multiple speed points must be used, it is necessary that the speeds span as wide a range as possible to give the best definition of the coefficients. This type of coefficient solution yields one general asymmetric set of constant stiffness and damping coefficients to fit the given data. In practice, however, these coefficients could vary appreciably with speed.

The second approach addresses this problem by assuming the rotordynamic coefficients to be skew-symmetric. For the type of fluid film element being investigated here, the fluid inlet is circumferentially uniform with 6 equally spaced, identical hydrostatic pressure pockets. The test bearing is also centered in its clearance space with no applied static load. These conditions dictate that the rotordynamic coefficients should be skew-symmetric (i.e., $K_{yy}=K_{zz}$, $K_{yz}=-K_{zy}$, and similarly for B and M). This reduces the number of unknowns so that the matrix equation for rotordynamic coefficients becomes:

$$\begin{bmatrix} b & h & a & g \\ -a & -g & b & h \\ h & -b & g & -a \\ -g & a & h & -b \end{bmatrix} \begin{Bmatrix} B_{yy}\omega \\ B_{yz}\omega \\ K_{yy}-M_{yy}\omega^2 \\ K_{yz}-M_{yz}\omega^2 \end{Bmatrix} = \begin{Bmatrix} m \\ n \\ p \\ q \end{Bmatrix} \tag{13}$$

where

ω = excitation frequency (rad/s)

Ω = shaft rotation frequency (rad/s) for all "synchronous only rigs" $\omega=\Omega$ always and all coefficients are functions of Ω.

Define:

$$K'_{yy} = K_{yy}-\Omega^2 M_{yy} \tag{14}$$

$$K'_{yz} = K_{yz}-\Omega^2 M_{yz} \tag{15}$$

Note that the two unknown inertia coefficients have been combined with the stiffness coefficients to form a combined pair of unknowns. Since there are now only four unknowns, the matrix solution can be carried out with data from a single speed. Also, the shaft speed has been placed in the unknown column vector instead of in the matrix elements.

The coefficients K_{yy}, K_{yz}, B_{yy}, B_{yz}, M_{yy}, and M_{yz} will, in general, vary with rotational speed Ω, and since only linear model characteristics are desired, they do not vary with excitation frequency ω. Tester data can be used with equation (13) to determine how K'_{yy}, K'_{yz}, B_{yy}, and B_{yz} vary with synchronous frequency $\omega=\Omega$. The damping terms are completely

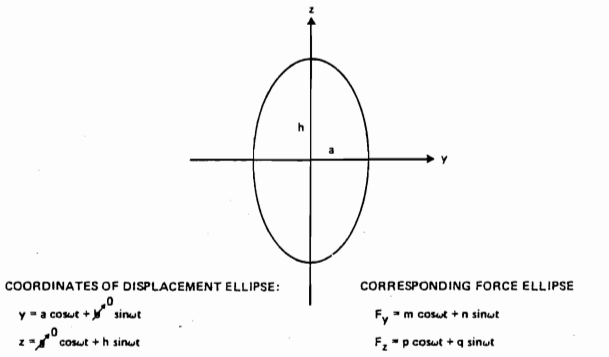

Fig. 4 Any displacement ellipse can be transformed through space and time into the above form without altering the skew-symmetric coefficient solution

separated from the stiffness terms without the need to vary tester speed. However, this requires that the fluid film displacement orbit be elliptic. If only circular orbits were possible, the above 4 by 4 matrix would become 2 by 2, and the stiffness and damping terms would need to be combined.

To show how such a separation is possible, and how effective this separation is, consider the displacement orbit shown in Fig. 4. Any displacement ellipse can be transformed into the ellipse of Fig. 4 without any loss in generality, and without altering the coefficient solution (a special result for the skew-symmetric coefficient arrangement). The same transformation is also enacted on the corresponding force ellipse. This transformation (in space and time) results in $b=g=0$ for the fluid film displacements, and establishes an easy solution for the unknown coefficients as follows:

$$B_{yy}\omega = -(an+hp)/(a^2-h^2) \tag{16}$$

$$B_{yz}\omega = (aq-hm)/(a^2-h^2) \tag{17}$$

$$K'_{yy} = (am-hq)/(a^2-h^2) \tag{18}$$

$$K'_{yz} = -(ap+hn)/(a^2-h^2) \tag{19}$$

It is now apparent that for a circular displacement orbit (i.e., $a=h$) the solution becomes undefined, and for a nearly circular orbit the solution is ill-defined. An adequate solution thus requires a sufficient amount of ellipticity in the displacement orbit.

A further understanding of this is gained by rearranging the above solution into a slightly different form:

$$B_{yz}\omega + K'_{yy} = (m+q)/(a+h) \tag{20}$$

$$-B_{yz}\omega + K'_{yy} = (m-q)/(a-h) \tag{21}$$

$$B_{yy}\omega + K'_{yz} = (p+n)/(-a+h) \tag{22}$$

$$-B_{yy}\omega + K'_{yz} = (p-n)/(a+h) \tag{23}$$

In this "sum and difference form", half of the solution is well defined even for circular orbits, while the other half is not. Synchronous excitation test rigs specifically designed to deliver circular orbits (e.g., see Childs et al.) can be used only to measure $(B_{yz}\omega+K'_{yy})$ and $(B_{yy}\omega-K'_{yz})$. The remainder of the solution cannot be identified from circular orbits. The quantity $(K'_{yy}+B_{yz}\omega)$ is sometimes referred to as net effective stiffness, and $(B_{yy}\omega-K'_{yz})/\omega$ as net effective damping.

An error analysis has been performed on the coefficient solution to quantify the sensitivity of the computed coefficients to experimental error as a function of the ellipticity ratio defined as follows:

$$\text{ellipticity ratio} = f = \frac{h}{a} \tag{24}$$

Small percentage changes in the data become excessively magnified during solution when f approaches one (i.e., when

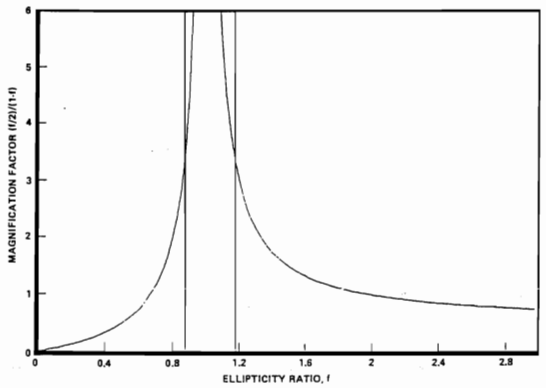

Fig. 5 Measurement error magnification factor for computed rotordynamic coefficients versus the relative displacement ellipticity ratio

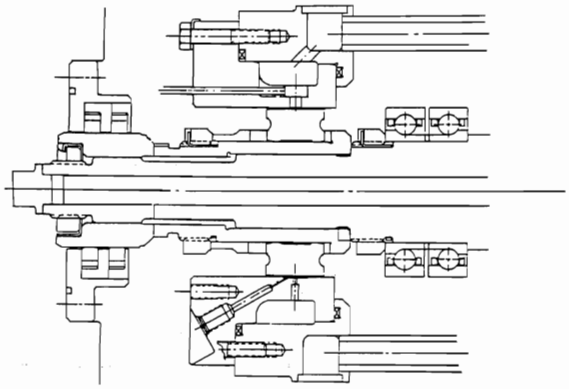

Fig. 6 Cross section of externally fed bearing. Freon flows right to left through flexure arms, and into stationary manifold.

the displacement orbit approaches a circle). As a function of f this error magnification is approximated as follows:

$$\text{error magnification} = \frac{(f/2)}{(1-f)} \tag{25}$$

Figure 5 shows this magnification plotted versus f. For the work reported here, f was required to be outside the range $.87 < f < 1.175$ so the magnification would be less than 3.5. When f is outside this range, stiffness and damping constants can be separated and quoted along with net effective values. When f is inside this range, only net effective stiffness and damping values can be obtained. With the test apparatus used here, the stator elastic support was made intentionally asymmetric, $K_{sy} \neq K_{sz}$, to generate the required ellipticity.

Testing Procedure. During data acquisition, the bearing supply pressure was held constant while the rotational speed was slowly ramped across the desired speed range at a rate of 200–500 rpm/s. The speed range of the tester operating in Freon was 0 to 22,700 rpm (378 Hz). the duration of any one test was limited to approximately one minute by the capacity of the Freon tank.

Analog data was stored on FM tape, then digitized and downloaded to a computer. Complex frequency spectrums were computed for each channel to provide synchronous Fourier coefficients. The frequency analysis was performed all along the speed ramp, essentially providing a sequence of snapshots at discrete values of tester speed.

Test Results. Testing was performed using Freon 113 at ambient temperature as the working fluid. Both an externally fed and an internally fed bearing configuration was tested (see Figs. 6 and 7). The dimensions of each configuration appear in Table 1.

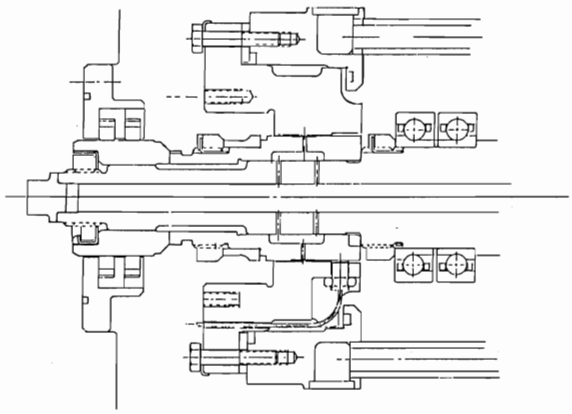

Fig. 7 Cross section of internally fed bearing. Freon flows right to left through hollow shaft, and outward into rotating manifold.

Table 1 Externally and internally fed hydrostatic bearing design description

Item		Internally Fed	Externally Fed
Bearing bore		54.61 mm	75.04 mm
Bearing length		25.4	25.4
Radial clearance		.0432	.0670
Orifice diameter		1.333	1.270
Orifice length		6.73	1.80
Recess description	Width (Circum)	8.18	11.41
	Length (Axial)	8.90	8.89
	Depth	.2032	.2286
	Surface recessed	Journal	Bearing
	Number of recesses	6	6
	Number of rows	1	1
	Area ratio	.10	.10

Table 2 Hydrostatic bearing test description

Test No. Item	8	10	28	31
Bearing type	External	External	Internal	Internal
Inlet pressure	3.4 MPag	10.3	10.3	10.3
Sump pressure	0 MPag	0	0	0
Radial clearance	.0432 mm	.0432	.0670	.0670
Eccentricity	.0064 mm	.0064	.022	.022
Temperature	309 K	312	296	295
Density	1540 kg/m3	1516	1579	1583
Flow rate	.39 kg/s	.61	.48	.47
Viscosity	.593 cp	.571	.708	.712
Load cells used	4	4	4	2
Ksy/Ksz	1.88	1.88	1.88	4.48
f>1.175	YES	YES	NO	YES

Two tests have been conducted for both the externally fed bearing and the internally fed bearing. The externally fed bearing tests were done with bearing inlet pressures of 3.4 and 10.3 MPa (500 and 1500 psig). All tests for all bearings shared the same sump pressure of 0 psig. The internally fed bearing tests had the same 10.3 MPa inlet pressure, but the first test produced insufficient ellipticity to permit separation of stiffness from damping via equation (13). For this reason, the second test of the internally fed bearing was conducted with two load cells replaced by eddy current displacement probes (F135 and F315 in Fig. 3). The load in that axis was identified by applying the stator displacement measured by the replacement probes to the measured stiffness of flexure tubes (shown in Figs. 1 and 2). This increased the stator support stiffness asymmetry ratio from 1.88 with 4 load cells, to 4.48 with 2 load cells. The increased support asymmetry resulted in sufficient ellipticity for the latter test of the internally fed bearing.

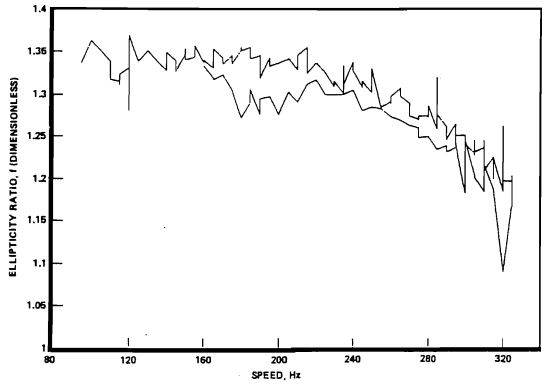

Fig. 8 Displacement orbit ellipticity ratio for the externally fed bearing at 10.3 MPa (test 10)

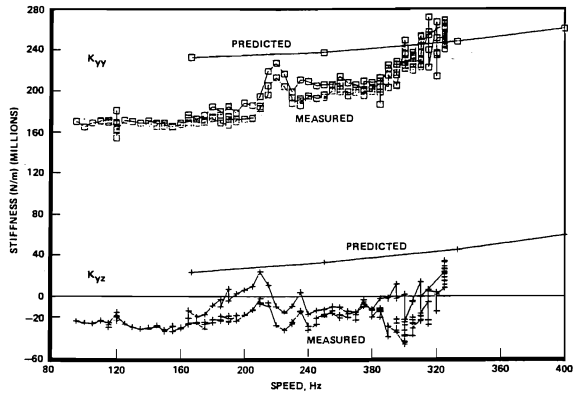

Fig. 9 Measured and predicted direct and cross-coupled stiffness coefficients for the externally fed bearing at 10.3 MPa (test 10)

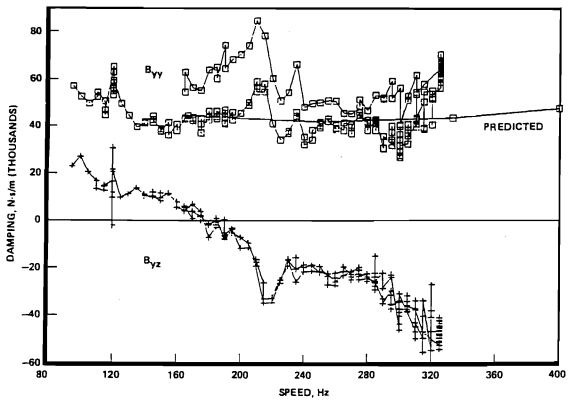

Fig. 10 Measured and predicted direct and cross-coupled damping coefficients for externally fed bearing at 10.3 MPa (test 10)

Externally Fed Bearing. The ellipticity ratio and the computed set of skew-symmetric rotordynamic coefficients are shown for both upramp and downramp in Figs. 8 thru 10 for the externally fed bearing operating with an inlet pressure of 10.3 MPa (see Table 2). Also shown in the figures are the predicted values for these coefficients obtained numerically with the computer program HBEAR described by Artiles et al. The ellipticity ratio is seen to satisfy the criteria of being greater than 1.175. Thus, separated stiffness and damping terms can be obtained. All measured coefficients exhibit the same trends versus speed as the predicted coefficients. The measured direct stiffness values are about 20 percent less than predicted, and the measured direct damping values are roughly equal to the predicted values. The measured cross-coupled stiffness is less than predicted, and is actually a stabilizing influence at low speed where $K_{yz} < 0$.

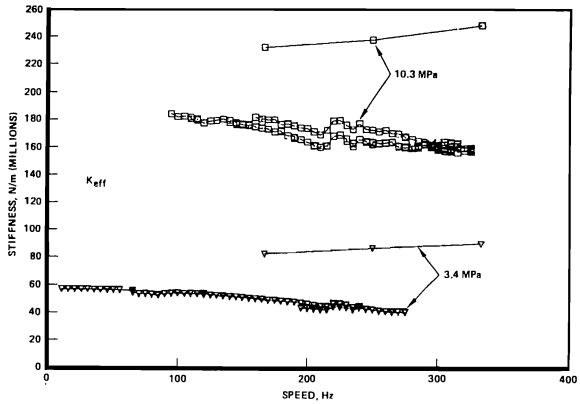

Fig. 11 Comparison of measured net effective stiffness for externally fed bearing with low and high inlet pressure (tests 8 and 10)

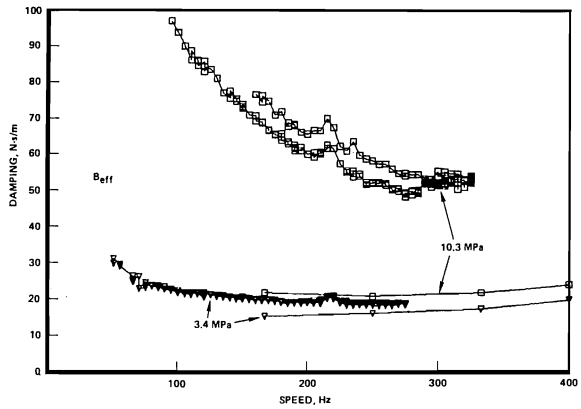

Fig. 12 Comparison of measured net effective damping for externally fed bearing with low and high inlet pressure (tests 8 and 10)

The analytical code does not predict cross-coupled damping, whereas the test measurements show what appears to be a significant amount of cross-coupled damping. It should be noted that one effect of cross-coupled damping is to either add to, or detract from, the apparent amount of asymmetry in the direct stiffness. The coefficient reduction method employed here assumes symmetric direct stiffness. One way asymmetry in the direct stiffness can manifest itself is by the prediction of nonzero cross-coupled damping coefficients. In this particular case, roughly 17.5 MN/m (100,000 lb/in.) of asymmetry could produce the type of cross-coupled damping coefficients shown.

Orbit ellipticity makes it possible to separate the stiffness from damping. If the orbits were too nearly circular, only net effective stiffness and damping defined by equations (20) and (23) could be determined. Figures 11 and 12 show a comparison of the measured and predicted net effective stiffness and damping values for the bearing of Figs. 8 thru 10. For use in analytical rotordynamic models, net effective values will suffice for performing unbalance response studies of symmetrically supported rotors, but they are less than ideal for performing rotordynamic stability studies, or for unbalance studies of asymmetrically supported rotors.

The bearing of Figs. 8 thru 12 was tested with a bearing inlet pressure of 10.3 MPa. The same bearing was tested with an inlet pressure of 3.4 MPa. Figures 13 thru 15 show the ellipticity ratio and comparisons of measured and predicted stiffness and damping. The data is similar to the data for 10.3 MPa except for the correspondingly lower magnitudes due to the lower inlet pressure. Also, agreement with the predictions is not as close as for the higher pressure. Figures 11 and 12 directly compare the net effective values, and show them to be very nearly proportional to inlet pressure.

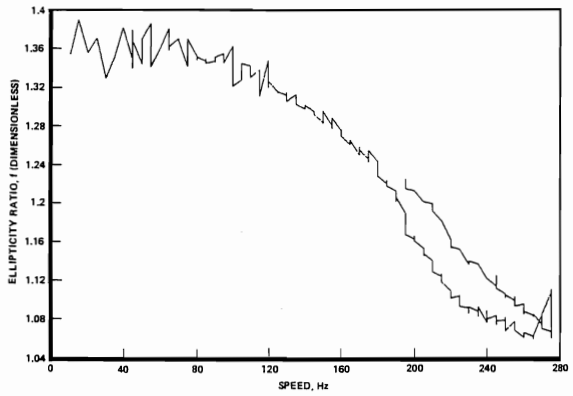

Fig. 13 Displacement orbit ellipticity ratio for externally fed bearing at 3.4 MPa (test 8)

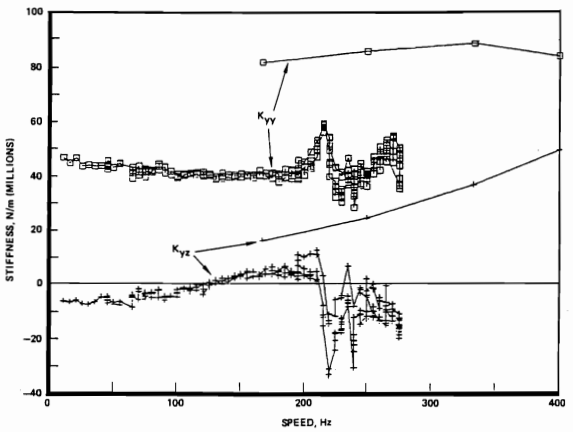

Fig. 14 Measured and predicted direct and cross-coupled stiffness for externally fed bearing at 3.4 MPa (test 8)

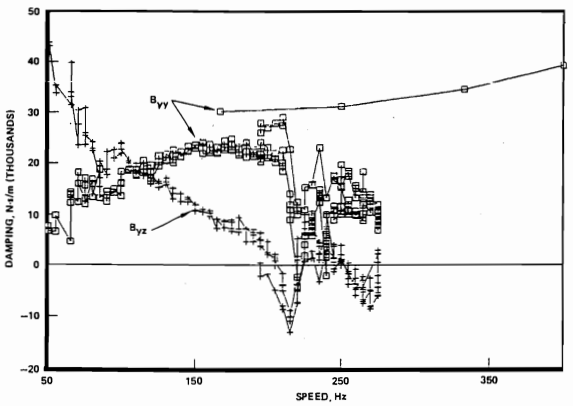

Fig. 15 Measured and predicted direct and cross-coupled damping for externally fed bearing at 3.4 MPa (test 8)

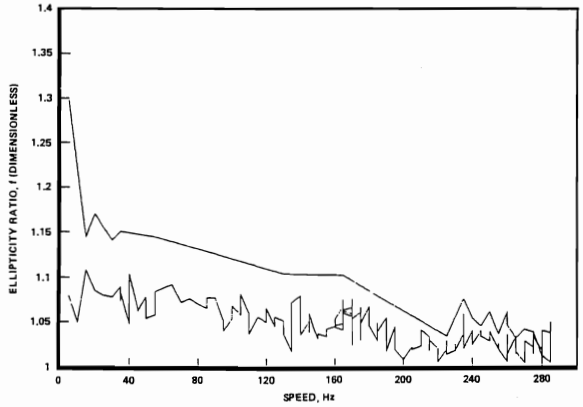

Fig. 16 Displacement orbit ellipticity ratio for internally fed bearing (test 28)

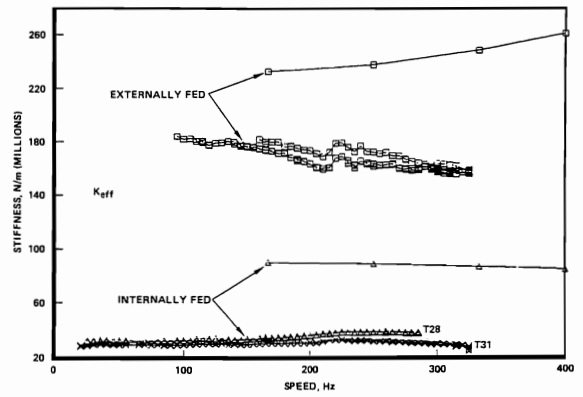

Fig. 17 Comparison of net effective stiffness for externally fed bearing (test 10) and internally fed bearing (tests 28 and 31)

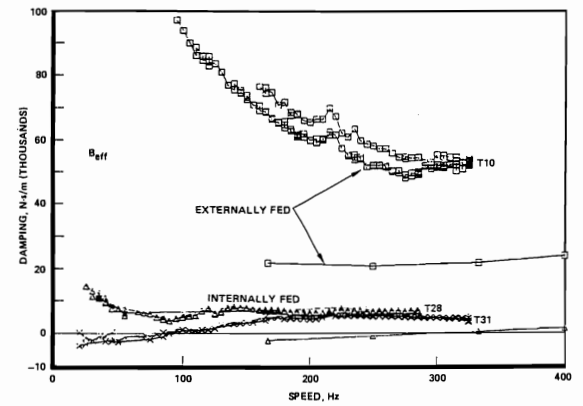

Fig. 18 Comparison of net effective damping for externally fed bearing (test 10) and internally fed bearing (tests 28 and 31)

In Fig. 13, note that as tester speed surpasses 200 Hz, the ellipticity ratio falls below the 1.175 criteria for separable data. As this occurs, the curves for the separated coefficients become more random (Figs. 14 and 15). Also note that the net effective values of Figs. 11 and 12 should not, and are not, affected by the orbit becoming too circular.

Internally Fed Bearing. In the first test of the internally fed bearing the ellipticity ratio was extremely close to 1, and thus only net effective values can be quoted. The cause for small ellipticity is that the internally fed bearing produces a much lower overall stiffness than the externally fed bearing, and thus generated less motion of the asymmetrically supported stator. It is forced motion of the stator that causes the relative orbits to be elliptic. Figures 16 thru 18 show the ellipticity ratio, and the measured and predicted net effective stiffness and damping for this test. The noted differences between predictions and measurements are qualitatively the same as the differences noted for the externally fed bearing. The net effective stiffness was overpredicted by 100 to 150 percent versus about 20 percent for the externally fed bearing. The net effective damping was both predicted and measured to be very small, and was underpredicted as it was for the externally fed bearing. Meaningful percentage differences cannot be quoted in this case as the measured and predicted values are of opposite sign.

Figures 19 thru 21 show the ellipticity ratio and all measured

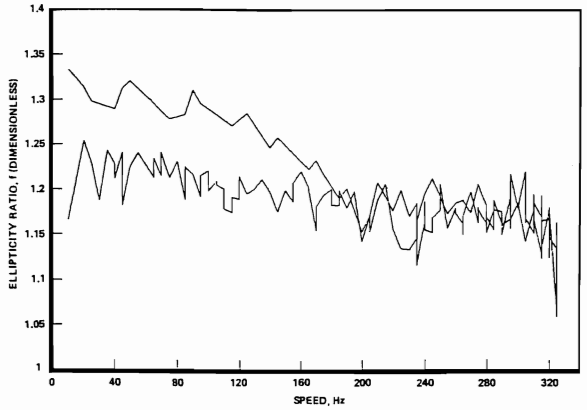

Fig. 19 Displacement orbit ellipticity ratio for internally fed bearing with two load cells (test 31)

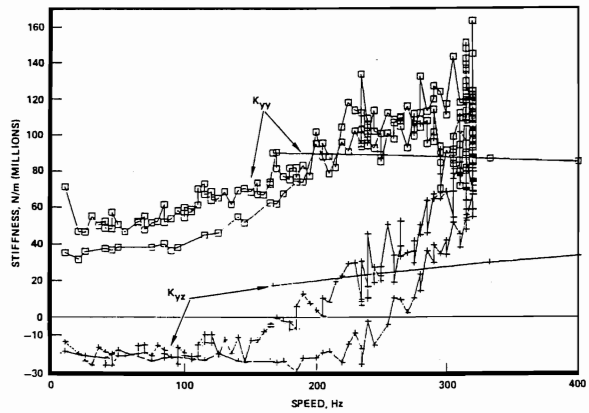

Fig. 20 Measured and predicted direct and cross-coupled stiffness coefficients for internally fed bearing with two load cells (test 31)

and predicted coefficients for the test of the internally fed bearing with two load cells removed. The separated stiffness and damping coefficients do not exhibit the qualitative agreement with predictions that the externally fed bearing shows. The measured and predicted direct stiffness actually agree quite well in magnitude near 220 Hz shaft speed, but the measurements show a major speed dependency contrary to predictions. The direct damping was measured to be negative at low speed, and it also shows a major speed dependency not predicted.

The net effective stiffness and damping values for this test compare favorably to those of the other internally fed bearing test, and had consistent correlation with theory.

Two potential causes exist for the prominent speed dependency exhibited in the skew-symmetric coefficients by the internally fed bearing:

(1) The effect of fluid tangential velocity induced by the rotating recesses may have more influence than predicted by the analysis.

(2) Although feeler-gage checks of the test bearing clearance indicated that the bearing was centered within .0076 mm (.0003 in.), misalignment of the stator with the shaft centerline will result in speed dependency for the skew-symmetric coefficients.

The data reduction process of equation (13) assumes the rotordynamic coefficients to be skew-symmetric. If, in fact, they are not skew-asymmetric, this condition can manifest itself in the data reduction process by causing the calculated skew-symmetric coefficients to vary with speed.

Speed Dependency Versus Asymmetry. If the data of the second internally fed bearing test is reduced according to the asymmetric method of equation (12), the following set of stiffness and damping values are produced:

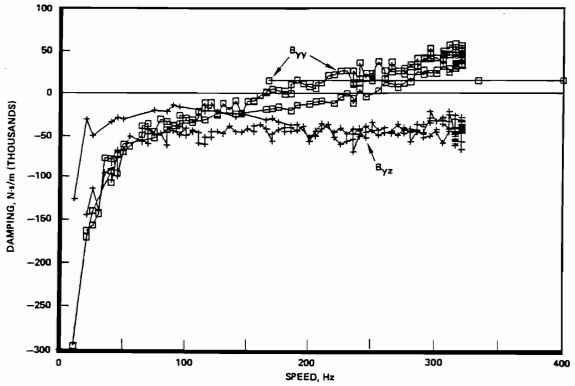

Fig. 21 Measured and predicted direct and cross-coupled damping coefficients for internally fed bearing with two load cells (test 31)

$$\begin{bmatrix} K_{yy} & K_{yz} \\ K_{zy} & K_{zz} \end{bmatrix} = \begin{bmatrix} 22.3 & 2.9 \\ -2.9 & 34.6 \end{bmatrix} \text{MN/m}$$

$$\begin{bmatrix} B_{yy} & B_{yz} \\ B_{zy} & B_{zz} \end{bmatrix} = \begin{bmatrix} -0.96 & 2.13 \\ -0.62 & 13.0 \end{bmatrix} \text{kN-s/m}$$

These values are dependent on the arbitrary orientation of the yz coordinate system. Stiffness and damping values computed for the yz coordinate system of Fig. 3 have been rotated to make the cross-coupled stiffness values of equal magnitude and opposite sign. In this case the required rotation is 28 degrees counterclockwise. The resulting direct stiffness values are different by a factor of 1.55, and the direct damping values are different by a factor of 13.5, and are of opposite sign.

The same procedure applied to the 10.3 MPa externally fed bearing test results in:

$$\begin{bmatrix} K_{yy} & K_{yz} \\ K_{zy} & K_{zz} \end{bmatrix} = \begin{bmatrix} 211 & 46 \\ -46 & 174 \end{bmatrix} \text{MN/m}$$

$$\begin{bmatrix} B_{yy} & B_{yz} \\ B_{zy} & B_{zz} \end{bmatrix} = \begin{bmatrix} 20.5 & 30.4 \\ -0.98 & 32 \end{bmatrix} \text{kN-s/m}$$

Asymmetry in the direct stiffness and damping is much less pronounced in this case with ratios of only 1.2 and 1.6, respectively.

Both reduction methods produce stiffness and damping values which serve to correlate the measured forces and displacements. Choosing between the two methods involves choosing between general asymmetry and speed dependency for the rotordynamic coefficients. One set of coefficients contains asymmetry, but is constant versus speed. The other set assumes skew-symmetry, but yields a direct measure of speed dependency. The choice must be dictated by which condition is expected to be most significant.

The predicted coefficients according to Artiles et al., in all cases, are skew-symmetric and vary with speed. Figures 9 and 10 show that the measured speed dependency parallels the predicted speed dependency for the 10.3 MPa externally fed bearing. The asymmetric coefficient set for this test also exhibits direct stiffness and damping which are very close in the y and z directions. Figures 20 and 21 for the internally fed bearing, however, show a dramatic difference between measured and predicted speed dependency for skew-symmetric coefficients. Also, the asymmetric coefficient set for this test shows large differences in the direct stiffness and damping.

Thus for the internally fed bearing, either the coefficients are approximately skew-symmetric and the measured speed dependency is real, or the coefficients are in reality asymmetric and the measured speed dependency in the skew-symmetric coefficients is part real and part due to asymmetry.

The only plausible source of significant coefficient asym-

metry is static miscentering of the stator about the bearing journal. The feeler gage checks already mentioned indicated that the bearing was centered within 12 percent of the clearance. Analysis of generic fluid film components has shown that miscentering must be as much as 40 percent of the clearance to produce significant asymmetry. Thus, the internally fed hydrostatic bearing may be more sensitive to miscentering than other types of fluid film elements.

Conclusion

Figures 17 and 18 show the net effective stiffness and damping for the three tests run at a common bearing supply pressure of 10.3 MPa. The internally fed bearing was physically smaller than the externally fed bearing, and also had larger clearance. Both these differences, which tend to lower the stiffness and damping, are accounted for in the predicted values. The most important aspects of a direct comparison of the internally versus externally fed configurations are as follows:

(1) Both configurations had measured net effective stiffness values which were lower than predicted, but the externally fed bearing was only 20% to 25% lower whereas the internally fed bearing was 60% lower.

(2) Both configurations had net effective damping values which were higher than predicted. The externally fed bearing was predicted, and shown, to have significant direct damping. The internally fed bearing analysis predicted low damping, and the bearing was subsequently shown to have practically neutral net effective damping.

The poor net effective damping qualities of the internally fed bearing are likely due to the fluid swirl condition. This condition results from the fact that the pressure pockets are rotating with the shaft. Fluid enters the bearing through holes in the pressure pocket recesses, and thus immediately has the full tangential velocity of the journal surface. Circumferential flow of this nature is known to have a detrimental effect on net effective damping. The damping performance on the internally fed bearing may be significantly enhanced by providing some type of circumferential flow attenuating device, or by giving the stator increased surface roughness, or both.

References

Artiles, A., Walowit, J., and Shapiro, W., 1982, "Analysis of Hybrid, Fluid Film Journal Bearings with Turbulence and Inertia Effects. Advances in Computer-Aided Bearing Design," Proceedings of ASME-ASLE Lubrication Conference, American Society of Lubrication Engineers, New York, N. Y., October

Childs, D. W., and Kim, C. H., 1982, "Analysis and Testing for Rotordynamic Coefficients of Turbulent Annular Seals with Different, Directionally Homogeneous Surface-Roughness Treatment for Rotor and Stator Elements," NASA Conference Publication 2338, Proceedings of the Workshop on Rotordynamic Instability Problems in High-Performance Turbomachinery, held at Texas A&M University, May 28–30.

Goodwin, M. J., Penny, J. E. T., and Hooke, C. J., 1985, "Hydrostatic Supports for Rotating Machinery — Some Aspects of Oil Film Non-Linearity," American Society of Mechanical Engineers, Paper No. 85-DET-123, Sept.